CARBON 49 (2011) 161–169

available at www.sciencedirect.com

ScienceDirect

journal homepage: www.elsevier.com/locate/carbon

Co-gelation synthesis of porous graphitic carbons with high surface area and their applications

Zhongli Wang, Xinbo Zhang, Xiaojuan Liu, Minfeng Lv, Kuiyue Yang, Jian Meng *

State Key Laboratory of Rare Earth Resource Utilization, Changchun Institute of Applied Chemistry, Chinese Academy of Sciences, Changchun 130022, PR China

ARTICLE INFO

Article history:
Received 25 June 2010
Accepted 31 August 2010
Available online 7 September 2010

ABSTRACT

An easy co-gelation route has been developed to synthesize porous graphitic carbons with high surface areas by using teraethylorthosilicate (TEOS), furfuryl alcohol (FA), and metal nitrates as precursors. Using a one-pot co-gelation process, a polyfurfuryl alcohol–silica interpenetrating framework with metal ions uniformly dispersed was formed during the polymerization of FA and the hydrolysis of TEOS within an ethanol solution of the three precursors. This synthesis process is simple and time-saving in comparison with the conventional preparation methods. During the heat treatment, Fe_7Co_3 alloy nanoparticles were produced by carbothermal reduction and they then catalyzed the graphitization of the amorphous carbon. The graphitic carbons obtained have a high crystallinity as shown by X-ray diffraction, Raman spectroscopy, and high-resolution transmission electron microscopy analysis. The degree of graphitization can be controlled by the varying the loading amount of catalyst. The porous texture of the carbons combines miropores and bimodal mesopores, mainly originating from the silica template formed with different sizes and the loose packing of the graphite sheets. The carbons have large surface areas (up to 909 m^2/g) and exhibit excellent electrochemical performance.

1. Introduction

Porous carbon materials have been recently attracted much attention due to their potential use in many emergent applications, such as gas storage, gas separation, as catalytic support, as specific adsorbents and as electrodes in electrochemical double layer capacitors or Li-ion batteries [1]. Optimal utilization of carbon materials in these fields depends to a large extent on their physical properties, which can be conveniently adjusted to the specific requirements of each application [2–9]. For this reason, in recent years a number of synthesis strategies have been developed to prepare porous carbons with controlled physical characteristics, such as pore size, particle size, morphology or porosity [10,11]. For certain application, it is the crystallinity of the carbon framework that plays a critical role. Specifically, porous graphitic carbon shows advantages over amorphous carbon because of the well-developed crystalline structure, high electronic conductivity and thermal stability and satisfactory oxidation resistance at low temperature as well [12,13]. Thus, synthesis of porous graphitic carbon with a large and accessible surface area is of great interest in the practical applications.

Nanostructured graphitic carbon materials, including carbon nanotubes, carbon nanofibers and carbon nanospheres, are usually produced under harsh conditions, such as arc discharge, laser evaporation and thermal chemical vapor deposition [14–16]. However, most of the materials synthesized by these techniques exhibit low surface area and low yield with a high proportion of impurities [13]. Conventional activating

* *Corresponding author:* Fax: +86 431 5689041.
E-mail address: jmeng@ciac.jl.cn (J. Meng).
0008-6223/$ - see front matter
doi:10.1016/j.carbon.2010.08.056

procedures, usually used to prepare activated carbons with high surface area, are not suitable for graphitic carbons, because these carbons are difficult to penetrate for gasifying agents, which presents the creation of pores. Heat treatment of porous carbon at the temperatures higher than 2000 °C is able to form well-developed graphitic structure, but such reaction conditions are rather energy and capital-intensive, in addition, they lead to a significant decrease in the surface area and pore volume of the porous carbon [17].

In order to avoid the high temperatures involved, transition metals have been used to catalyze the graphitization of amorphous carbon at lower temperatures. Many groups have been working on metal-doped carbon aerogels for catalysis, adsorption and electrode materials. For example, Baumann's group have prepared carbon aerogels doped with cobalt or nickel through sol–gel polymerization of formaldehyde with the potassium salt of dihygroxybenzoic acid, followed by ion exchange with $M(NO_3)_2$ (where $M = Co^{2+}$ or Ni^{2+}), and after the samples pyrolyzed at 1050 °C, the growth of graphitic nanoribbons with different curvatures is observed [18,19]. Moreno-Castilla's group prepared graphitized domains with three-dimensional stacking order by heating Cr-, Fe-, Co-, or Ni-doped carbon aerogels higher than 1000 °C [20]. Hyeon's group synthesized carbon nanocoils by heat treating composites made up of resorcinol–formaldehyde gel, silica, and transition-metal salts, followed by washing with NaOH solution and HNO_3 solution to remove silica and metal particles [21]. Recently, by using cobalt nanoparticles as the sacrificial template and cetyltrimethylammonium bromide as the surfactant and carbon source, Schuth's group fabricated a graphitic hollow shell after pyrolysis at 850 °C and following leaching of the cobalt nanoparticles by acid solution [22]. However, the above synthetic processes are rather time-consuming and in most cases cannot be applied for large-scale for practical applications. Therefore, the exploration of simple and scalable synthetic procedure for porous graphitic carbon is of great interest.

It is well-known that the sol–gel technique is a useful method to prepare organic and inorganic materials [23–25]. In this paper, we developed an easy co-gelation sol–gel route for the synthesis of porous graphitic carbons by using three kinds of precursor containing FA, TEOS, and metal nitrates. FA and TEOS were simultaneously polymerized within an ethanol solution of FA, TEOS, and metal nitrates, which produced polyfurfuryl alcohol–silica interpenetrated organic–inorganic hybrid gels, accompanying the participation of metal salts. A mixture of iron and cobalt salts was decomposed and in situ carbonthermal reduced into alloy nanoparticles which catalyze the formation of the graphitic carbon. The TEOS was hydrolyzed to form interconnected silica network which acted as a hard template for porous carbons. The advantage of this method is that two processes of the formation of silica template and dispersion of catalyst were simultaneously carried out in one co-gelation process, which makes the synthesis very simple and eliminates the time-consuming synthesis of the silica template. The porous carbons have large surface areas and pore volumes. The degree of graphitization can be controlled by varying the loading amount of metal salts. In addition, such graphitic porous carbons were successfully applied to supercapacitors and exhibited excellent capacitive performance with high-rate response and low electronic resistance.

2. Experimental

2.1. Synthesis

Porous graphitic carbon materials were prepared by co-gelation of FA, metal nitrates and TEOS at 40 °C and 80 °C, followed by a carbonization treatment at 900 °C under inert gas and removing silica and catalyst in HF solution. In a typical preparation, 1 mmol metal nitrates (0.7 mmol $Fe(NO_3)_3{\cdot}9H_2O$ and 0.3 mmol $Co(NO_3)_2{\cdot}6H_2O$) was dissolved in 1 ml ethanol, followed by mixing with 1 g furfuryl alcohol. After stirring for 15 min, 2 g TEOS was added into the mixture. After stirring for another 30 min, red solution was obtained in a beaker. It took 12 h at 40 °C and 8 h at 80 °C in a water bath for the thermopolymerization and sol–gel process. The xerogel was carbonized at 900 °C for 2 h with a ramping rate of 2 °C/min under nitrogen flow. Then the black xerogel composite was treated with 48% HF solution. The final product was denoted as PGC-1.

The same procedures were carried out for the preparation of samples PGC-1.5 and 2, except that the amounts of metal nitrates were 1.5 mmol and 2 mmol, keeping the molar ration of $Fe(NO_3)_3{\cdot}9H_2O$ and $Co(NO_3)_2{\cdot}6H_2O$) to 7:3, for PGC-1.5 and 2, respectively.

2.2. Characterization

Thermogravimetric analysis (TGA) was carried out using a Mettler Toledo TGA-SDTA851 analyzer (Switzerland) from 25 °C to 1000 °C in a air flow of 80 ml/min at a heating rate of 5 °C/min. Wide-angle XRD patterns were collected on Bruker D8 Focus Powder X-ray diffractometer using Cu Kα radiation (40 kV, 40 mA). The energy-dispersive X-ray (EDX) spectra were performed by using a field emission scanning electron microscopy (HITACHI S-4800). TEM and HRTEM images were taken on a FEI Tacnai G2 electron microscope operated at 200 kV. For TEM measurements, the samples were prepared by dispersing the powder products as slurry in ethanol and drying on a holey carbon film on a Cu grid for measurements. N_2 adsorption–desorption isotherms were measured with a Micromeritics 2020 analyzer at 77 K. Before measurements, the samples were degassed at 150 °C for more than 5 h. The Brunauer–Emmett–Teller (BET) method was utilized to calculate the specific surface areas. The pore size distributions were derived from the desorption branches of the isotherms based on the Barrett–Joyner–Halanda (BJH) model. The total pore volume was estimated from the amount adsorbed at a relative pressure (P/P_0) of 0.99.

2.3. Electrochemical measurement

The working electrode was prepared by mixing 80 wt.% active materials (PGC), 10 wt.% acetylene black, and 10 wt.% polytetrafluoroethylene with ethanol to form slurry, and spreading onto a nickel-foam (1 cm^2). The mass load of active material on electrode was about 5 mg/cm^2. The electrochemical performance was characterized by cyclic voltammetry (CV) and

electrochemical impedance spectroscopy (EIS). The electrolyte was 6 mol L^{-1} KOH solutions. The measurement was carried out in a three-electrode cell, with nickel-foil counter electrode and Hg/HgO reference electrode. The data was acquired using CHI 660A electrochemical system. The CV experiments was conducted in the potential range of −0.8 to 0.2 V vs. Hg/HgO with potential sweep rates from 5 mV/s to 200 mV/s. The ESI experiment was performed with a bias potential of 0 V vs. Hg/HgO, amplitude of 10 mV, and a frequency range from 100 kHz to 10 mHz.

3. Results and discussion

The overall synthesis for preparing porous graphitic carbon is schematically illustrated in Fig. 1. There are three steps in the preparation process including co-gelation, carbonization and HF etching. The photographs of products at different stages are shown in Fig. S1. The key step in the current synthetic procedure is the simultaneous polymerization of carbon precursor (furfuryl alcohol) and silica precursor (TEOS) to produce homogeneous organic–inorganic hybrid gels within an ethanol solution containing TEOS, FA, and metal nitrates. Usually, HCl solution is needed for the hydrolysis of TEOS and the polymerization. But in this synthesis strategy, the solution containing metal nitrates instead of HCl solution provides weak acid media, especially for the iron nitrate solution. With the ethanol evaporating and the solution contacting, the acidity gradually increased and the simultaneous polymerization

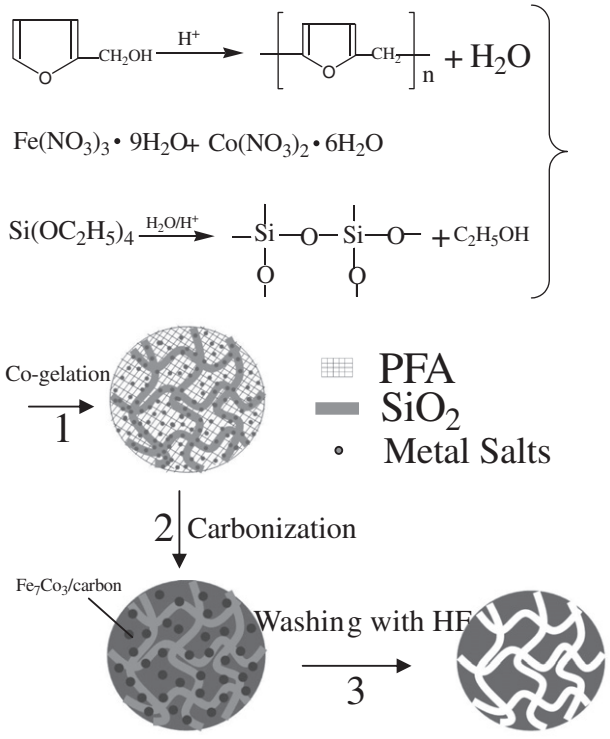

Fig. 1 – Illustration of the synthesis for the PGCs obtained from FA, TEOS, and metal nitrates. (1) Co-gelation of three kinds of precursors through polymerization and hydrolysis; (2) carbonization of xerogel in nitrogen; (3) washing silica and catalyst with HF solution.

was initiated. During the co-gelation sol–gel process, a phrase separation between PFA and silica took place on nanometer scale due to their different reaction rates, the former of which was faster than the latter at the present condition. As a result, PFA and silica network were formed, respectively. However, reactions between silanol groups and alcohols or carbocations of PFA sequences occurred to form Si–O–C bonds at the same time, which facilitated the formation of PFA–silica interpenetrating organic–inorganic hybrid frameworks [26–29]. Porous silica and carbon (Fig. S2) could be obtained by treating the hybrid gel with calcination in air and carbonization in N_2, respectively, which confirmed the above analysis. As an important component, metal salts participated in the whole co-gelation process and could interact with PFA and TEOS by forming organic polymer gel and inorganic silica gel, respectively. After carbonization in N_2 atmosphere (step 2), the XRD patterns of three composites (Fig. S3) exhibit diffraction peaks of Fe_7Co_3 alloy (JCPDS 48-1816) and graphite (JCPDS 41-1487). During the process of carbonization, Fe_7Co_3 alloy nanoparticles were firstly produced by in situ carbonthermal reduction of the mixed metal oxides and then catalyzed the amorphous carbon to form graphite according to a dissolution–precipitation mechanism [30,31]. From the TEM images of three composites (Fig. S4), it was clearly observed that Fe_7Co_3 alloy nanoparticles were uniformly dispersed in the carbon/silica matrix and were still remained in the porous carbon after removing silica in NaOH solution, which indirectly illustrated the uniform dispersion of metal ions in the hybrid gel. The content of alloy relative to carbon were measured by the EDX analysis and listed in Table 1. In step 3, the final porous graphitic carbons were obtained after washing the silica framework and alloy catalyst in HF solution. The particle sizes of graphitic carbons ranged from several hundred nanometers to several micrometers (Fig. S1e).

XRD patterns of the PGC samples are shown in Fig. 2. They exhibit well-resolved XRD peaks at 26°, 43°, 54°, and 78°, which are assigned to the (0 0 2), (1 0), (0 0 4) and (1 1 0) diffractions of the graphitic framework, respectively, according to the JCPDS Card Number 41-1487. A sharp (0 0 2) peak is associated with a high graphitic character as compared to a broad diffuse peak seen in amorphous carbon. With increasing the loading of catalyst, the (0 0 2) peak becomes sharper and narrower, indicating an increase in the degree of graphitization. The crystallite sizes of graphite measured perpendicular to the basal plane (L_c) were calculated from the (0 0 2) reflections, using Scherrer formula, $L_c = 0.89\lambda/B\cos(\theta)$, where λ is the wavelength of the X-ray (1.54 A), B is the full angular width at half max, and θ is the Bragg angle. The monotonic increase in the values of L_c (Table 1) with increasing the amount of metal salts indicates progressive graphitization of the carbon. The graphitic carbons obtained by using different catalysts were also compared by the XRD patterns (Fig. S5). From the strength of diffraction peaks, it can be seen that Fe_7Co_3 alloy exhibits best performance of catalysis than the single metal Fe, Co or other alloys at the same conditions, which indicates the ratio of ion to cobalt has effect on the activity of catalysis. Carbonization temperature is another factor which affects the degree of graphitization. As shown in Fig. S6, the peaks of graphite become sharper with increasing the carbonization temperature.

Table 1 – Catalyst content and structure parameter of the porous graphitic carbons.

Sample	Catalyst content (%)	Lc[a] (nm)	L_a[b] (nm)	Surface area (m2/g)	Pore volume (cm^3/g)	Pore size (nm)
PGC-1	7.4	7.8	2.1	909	0.73	2, 3.5, 8
PGC-1.5	13.8	9.2	3.1	698	0.78	2, 3.7, 10
PGC-2	18.2	10.4	3.7	593	0.74	2, 3.9, 12

[a] L_c is calculated from the (0 0 2) reflection of XRD patterns by using Scherrer formula.
[b] L_a is calculated from the Raman spectra by using formula $L_a = 4.4/(I_D/I_G)$.

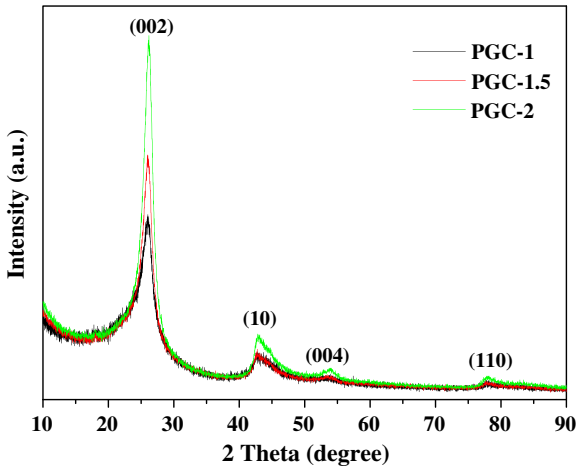

Fig. 2 – XRD patterns of the porous graphitic carbons obtained with different loading amount of catalyst.

The first order Raman spectra for PGC-1, 1.5 and 2 are shown in Fig. 3. There are two apparent peaks in the spectra for all three samples, corresponding to the D band at 1355 cm^{-1} and the G band at 1583 cm^{-1}. The D band is often referred to as the "disorder" band and is commonly believed to be a Raman inactive mode that becomes active as the disorder in the system is increased, or likewise as the symmetry at or near a crystalline edge is reduced [32,33]. The G band is present in all sp^2 hybridized carbon materials and arises from the E_{2g} vibrational mode. By determining the area under the peak for the D band and the G band, I_D/I_G (ratio of amorphous to graphitic carbon) values were estimated to be 2.1, 1.4, and 1.2 for PGC-1, 1.5 and 2, respectively. The values of I_D/I_G decreases with increasing the amount of metal salts, indicating the improving degree of graphitization. The relative levels of graphitization can be discerned by estimating the in plane crystalline length, $L_a = 4.4/(I_D/I_G)$ [34]. As the I_D/I_G ratio decreases, L_a increases from 2.1 nm to 3.7 nm for PGC samples, which indicates the growth in size of graphitic crystallites with increasing the amount of catalyst.

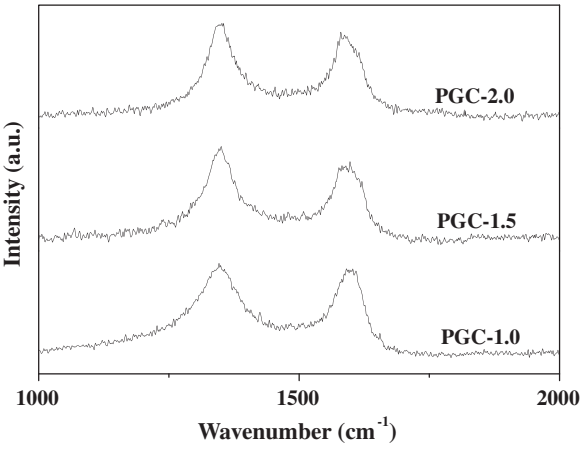

Fig. 3 – Raman spectra of the porous graphitic carbons obtained with different loading amount of catalyst.

To obtain more detailed structural insight, the samples were investigated by TEM analysis (Fig. 4). It can be seen that foamlike graphite structures with a disordered porosity made up of mesopores and micropores were produced. The curved graphitic sheets become more and more obvious with increasing catalyst amount, indicating the improvement of graphitization. At the same time, the pore sizes of void between graphite sheets gradually become large from PGC-1 to PGC-2. The fringes of the graphite crystallite were distinctly presented on all HRTEM images shown in Fig. 4d–f that were taken throughout the sequence of samples from PGC-1 to PGC-2. Layered ribbon-like graphitic structures are evident. The black lines in the layers are individual graphene planes. The significant amount of graphite ribbons in the carbon increase from PGC-1 to PGC-2, indicating the increase of graphitization, in accordance with the XRD results. Electron diffraction patterns of selected graphitized areas (inset of Fig. S7a–c) further reveal the crystallinity of three samples. The thickness of ribbons measured from TEM increases monotonically as 7.4 nm, 9.7 nm, and 10.8 nm, for PGC-1, 1.5 and 2, respectively, which is in good agreement with the L_c values estimated from XRD data. The distance between graphite layers (0 0 2) was measured to be ~0.34 nm from HRTEM images (Fig. S7d–f) which is larger than the typical value of graphite, suggesting that the stacking of graphene layers has experienced some distortion (turbostratic structure) [18]. The graphitic carbon is mainly produced from the amorphous carbon which is in contact with the catalyst nanoparticles, so all the shape of graphitic ribbons exhibit cycle-like structures with different curvature.

Fig. 5 shows the N_2 adsorption–desorption isotherms and the corresponding BJH pore size distribution of the as-prepared graphitic porous carbons, and the BET surface areas and the pore volumes of the samples are summarized in Table 1. Three samples have type IV isotherms with H1 hysteresis. The general shape of the N_2 sorption isotherms indicates that the as-prepared carbon materials contain multimodel pores. The initial vertical part of the curve at low relative pressure reveals the presence of micropores. The adsorbed volume at low relative pressure gradually decrease from PGC-1 to PGC-

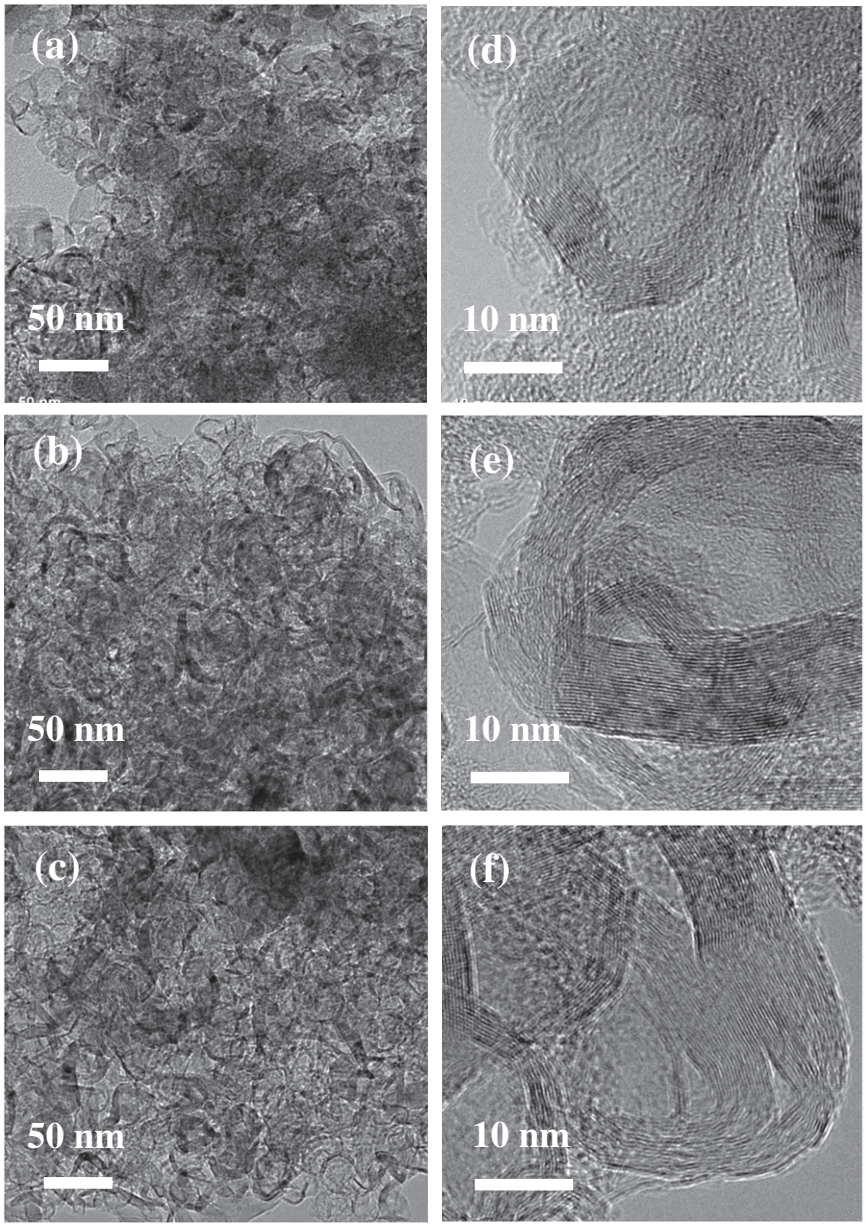

Fig. 4 – TEM and HRTEM images of the porous graphitic carbons: (a) and (d) of PGC-1; (b) and (e) of PGC-1.5; (c) and (f) of PGC-2.

2, indicating the micropore volume gradually decrease, while the size of hysteresis loops gradually becomes bigger, indicating the mesopore volumes gradually increase. The surface areas are 909 m^2/g, 698 m^2/g, and 593 m^2/g, for PGC-1, 1.5, and 2, respectively, decreasing with the increase of graphitization. In contrast, the total pore volumes are almost not changed, suggesting the increase of pore size from PGC-1 to PGC-2. The corresponding pore size (Fig. 5b) can further illustrate the above results. There are three pore size distributions, the first of which is micropores (<2 nm), the second is mesopores centered at 4 nm and the last is mesopores with sizes varying as 8 nm, 10 nm, and 12 nm, for PGC-1, 1.5, and 2, respectively. The dissolution of silica framework and loose packing of graphite sheets resulted in such hierarchical porous structures, which will facilitate the mass diffusion during the practical applications. Obviously, the micropore volumes gradually decrease from PGC-1 to PGC-2, while the mesopore volumes gradually increase, which is in good agreement with the adsorption curves. Similar phenomenon was also observed in the samples prepared by carbonizing the precursor xerogel of PGC-1.5 at different temperatures. Although they had same initial PFA–silica interpenetrated framework, the pore structures of carbons still varied regularly with the degree of graphitization (Fig. S8 and Table S1). Such changes of pore structures with the difference of graphitization can be explained by the process of graphitization as illustrated in Fig. 6. When irregular amorphous carbon was converted into regular graphitic carbon within the silica template, the volume of carbon shrank and large void was produced, which could be observed in the TEM images of Fe_7Co_3/carbon/silica composites before HF treatment (Fig. S9). Before graphitization, silica template introduced micropores in amorphous

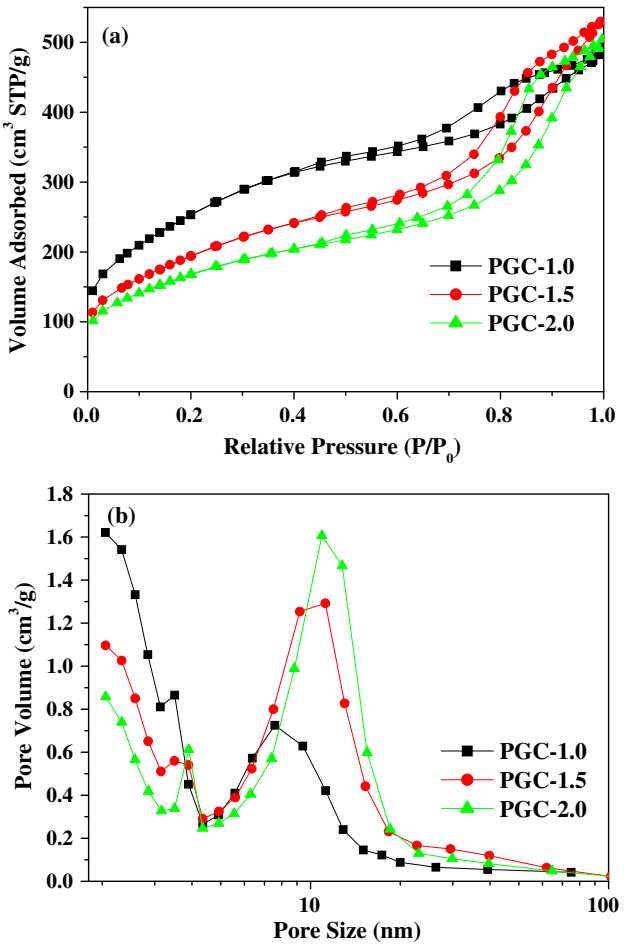

Fig. 5 – Nitrogen sorption isotherms (a) and pore size distribution curves (b) of porous graphitic carbons with different loading amount of catalyst.

carbon, but after graphitization and removing template, micropores and void coalesced and pore sizes became large, which lead to the decrease of micropores and the increase of mesopores.

It is well-known that graphitized carbons with a higher graphitization degree are more stable against air oxidation. To study the resistance of the PGC samples, TGA analysis were performed under air to examine the oxidation behavior of these porous carbons. As seen in Fig. 7, PGC-1 is more rapidly oxidized compared to the PGC-2, that is, the lower graphitized carbon is easily oxidized with oxygen. The oxidation temperature for PGC-2 increases 50 °C compared to the PGC-1. Graphitic carbon prepared with high loading of catalyst shows better oxidation resistance than the one prepared with low loading, which is due to the different graphitization degree of these carbons [35].

CV measurements were conducted to test the supercapacitor performances of the PGC samples. Fig. 8 presents the capacitive behaviors of the samples and their CV profiles were investigated at different scan rate from 5 mV/s to 200 mV/s between −0.8 V and 0.2 V in 6 M KOH aqueous electrolyte by using a three-electrode cell. It can be observed that all the carbons present a rectangular voltammogram shape at the whole voltage window, indicating of excellent candidates as electrode materials for electrochemical double layer capacitor. As the scan rate increased, the CV curves became gradually depressed but still maintained a less rectangular shape, which means that the PGC samples would be suitable for quick charge–discharge operations [36,37]. In comparison, at low scan rate the CV curve shapes of the three samples were typically rectangular, but at high scan rate the curve of PGC-1 showed a slow change at the switching potential due to its much smaller pore size and the low utilization of surface area.

The capacitance of the porous carbon materials can be estimated by the equation of $C_g = [i(dt/dv)]/m$, where C_g is the differential capacitance, i is the current in the cyclic voltammogram, and m is the mass of the active materials [38–40]. The capacitance of different scan rates calculated from the middle voltage of −0.3 V in Fig. 8 are listed in Table 2. The calculated capacitances of three samples are 118 F/g, 90 F/g, and 77 F/g, for PGC-1, 1.5 and 2, respectively. It is superior to graphitized CMK-3 materials derived from anthracene, for example, which display values of 20–60 F/g [41,42]. The relationship between the retained capacitance ratio and volt-

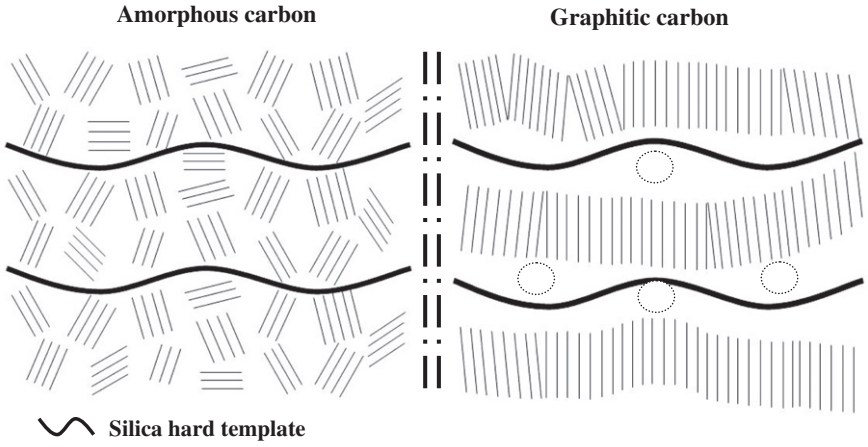

Fig. 6 – Illustration of the graphitization process from amorphous carbon to graphitic carbon within the silica hard template, accompanying large void produced (circles).

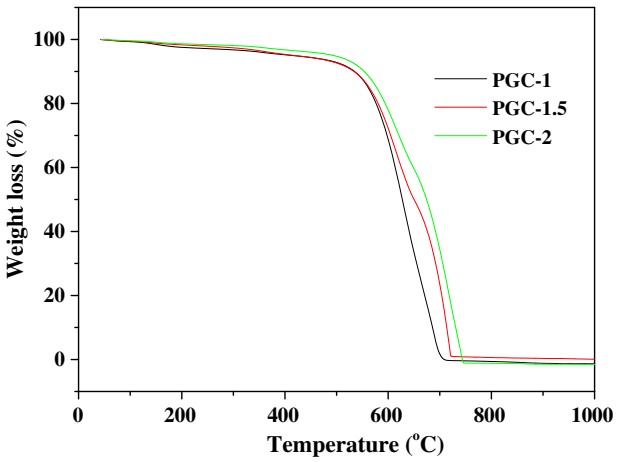

Fig. 7 – TGA curves of the porous graphitic carbons with different loading amount of catalyst.

age scan rate is plotted in Fig. 8d. Obviously, the high retained ratios were obtained for three samples and increase monotonically as 80%, 84%, and 86%, for PGC-1, 1.5 and 2, respectively. These results highlight the suitability of PGC samples for high-rate operation. It can be seen that micropores increase the capacitance as for PGC-1, while the mesopores favor the fast ionic motion and increase the ion response. Therefore, a well-balanced micro/mesoporosity is helpful to improve the performance of supercapacitors.

The EIS analysis has been recognized as one of the principal method for examining the fundamental behavior of electrode materials for a supercapacitor. As shown in Fig. 9, the impedance plots exhibit two distinct parts including a semicircle in the high-frequency region and a sloped line in the low-frequency region. The resistance of a supercapacitor, namely equivalent series resistance or ESR, consists of electronic contributions and ionic contributions [43]. It can be seen that the ESR of three samples are all low values and decrease monotonically as 0.25 Ω, 0.17 Ω, and 0.11 Ω, for PGC-1, 1.5 and 2, respectively, which suggests the electronic resistance and ionic diffusion resistance decrease from PGC-1 to 2, in accordance with the CV results. The ESR results further reveal that the graphitization improved electronic conductivity and large pore size increased the diffusion efficiency. In addition, at the low-frequency region, the slope of PGC-2 is

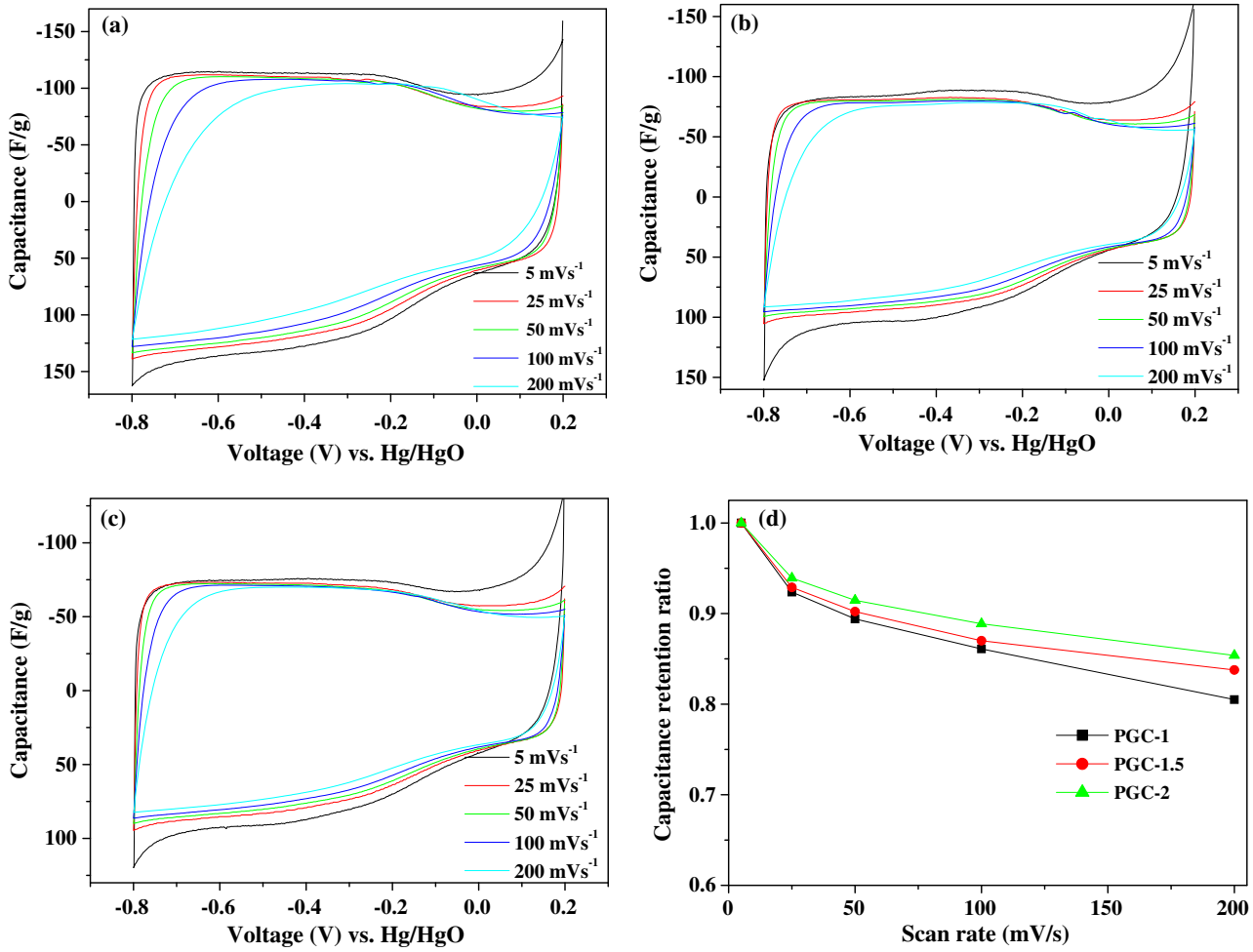

Fig. 8 – CV curves of (a) PGC-1, (b) PGC-1.5, and (c) PGC-2 at different scan rates in 6 M KOH electrolyte by using a three-electrodes configuration, the capacitance is based on the weight of active materials in working electrode. (d) Capacitance retention ratio as a function of the potential sweep rates.

Table 2 – Capacitances of the porous graphitic carbons obtained by the data of CV measurements in Fig. 8.

Scan rate (mV/s)	5	25	50	100	200
PGC-1 capacitance (F/g)	118	109	106	102	95
PGC-1.5 capacitance (F/g)	90	84	81	78	75
PGC-2 capacitance (F/g)	77	73	71	69	65

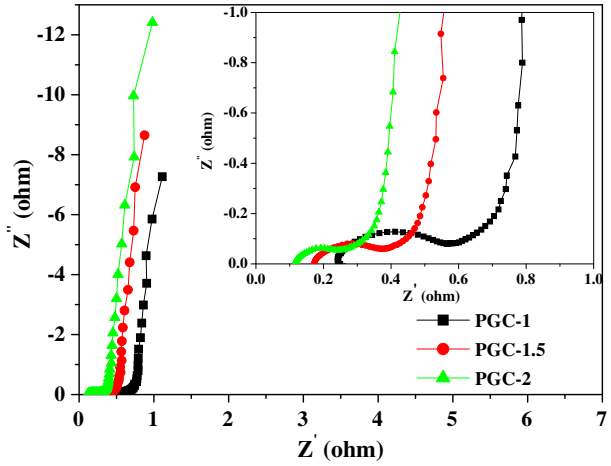

Fig. 9 – Nyquist plots for the porous graphitic carbons in 6 M KOH electrolytes recorded at room temperature with a frequency range from 100 kHz to 10 mHz.

steeper than the others, which indicates the better capacitive performance [44].

4. Conclusions

The porous graphitic carbons with high surface areas have been successfully synthesized by an easy co-gelation sol–gel route using TEOS, FA, and metal nitrates as precursors. By the one-pot co-gelation process, PFA–silica interpenetrating framework with metal ions uniformly dispersed was formed during the polymerization of FA and the hydrolysis of TEOS within an ethanol solution of three precursors. This synthesis process is simple and time-saving in comparison with the conventional preparation methods. During the heat treatment, Fe_7Co_3 alloy nanoparticles were produced by in situ carbonthermal reduction and then catalyzed the graphitization of amorphous carbon. The graphitic carbons obtained have a high crystallinity as evidenced by XRD, Raman spectra, and HRTEM analysis. The degree of graphitization can be controlled by the varying the loading amount of catalyst. The porous texture of the carbons combines miropores and bimodal mesopores, mainly originating from the silica template formed with different sizes and the loose packing of graphite sheets. The porous graphitic carbons have large surface areas (up to 909 m^2/g) and pore volumes (up to 0.78 cm^3/g). The electrochemical properties as an electrode material for supercapacitor applications were investigated in aqueous electrolyte. They showed rectangular-shaped cyclic voltammetry curves with large capacitances (up to 118 F/g) over a wide range of scan rates even as high as 200 mV/s, and exhibited fast ion response with high capacitance retention ratio (up to 86%). The excellent electrochemical performance can be attributed the hierarchical porous structures which improve the electronic conductivity and ionic diffusion efficiency of the carbon materials.

Acknowledgement

This project was supported by National Natural Science Foundation of China (Grant Nos. 20831004 and 20771100).

Appendix A. Supplementary data

Supplementary data associated with this article can be found in the online version, at doi:10.1016/j.carbon.2010.08.056.

REFERENCES

[1] Burchell TD. Carbon materials for advanced technologies. Amsterdam: Pergamon Press; 1999.
[2] Sevilla M, Salinas Martinez-de Lecea C, Valdes-Solis T, Morallon E, Fuertes AB. Solid-phase synthesis of graphitic carbon nanostructures from iron and cobalt gluconates and their utilization as electrocatalyst supports. Phys Chem Chem Phys 2008;10:1443–52.
[3] Wang DW, Li F, Chen ZG, Lu GQ, Cheng HM. Synthesis and electrochemical property of boron-doped mesoporous carbon in supercapacitor. Chem Mater 2008;20:7195–200.
[4] Padilla-Serrano MN, Maldonado-Hodar FJ, Moreno-Castilla C. Influence of Pt particle size on catalytic combustion of xylenes on carbon aerogel-supported Pt catalysts. Appl Catal B Environ 2005;61:253–8.
[5] Duarte F, Maldonado-Hodar FJ, Perez-Cadenas AF, Madeira LM. Fenton-like degradation of azo-dye Orange II catalyzed by transition metals on carbon aerogels. Appl Catal B Environ 2009;85:139–47.
[6] Catalao RA, Maldonado-Hodar FJ, Fernandes A, Henriques C, Ribeiro MF. Reduction of NO with metal-doped carbon aerogels. Appl Catal B Environ 2009;88:135–41.
[7] Mariea J, Chenitza R, Chatenet M, Berthon-Fabrya S, Cornet N, Acharda P. Highly porous PEM fuel cell cathodes based on low density carbon aerogels as Pt-support: experimental study of the mass-transport losses. J Power Sources 2009;190:423–34.
[8] Marie J, Berthon-Fabry S, Achard P, Chatenet M, Pradourat A, Chainet E. Highly dispersed platinum on carbon aerogels as supported catalysts for PEM fuel cell-electrodes: comparison of two different synthesis paths. J Non-Cryst Solids 2004;350:88–96.
[9] Fu RW, Lin YM, Rabin O, Dresselhaus G, Dresselhaus MS, Satcher Jr JH, et al. Transport properties of copper-doped carbon aerogels. J Non-Cryst Solids 2003;317:247–53.
[10] Moreno-Castilla C, Maldonado-Hodar FJ, Rivera-Utrilla J, Rodriguez-Castellon E. Group 6 metal oxide–carbon aerogels: their synthesis, characterization and catalytic activity in the

skeletal isomerization of 1-butene. Appl Catal A: Gen 1999;183:345–56.
[11] Liu HJ, Jin LH, He P, Wang CX, Xia YY. Direct synthesis of mesoporous carbon nanowires in nanotubes using MnO_2 nanotubes as a template and their application in supercapacitors. Chem Commun 2009:6813–5.
[12] Lu AH, Li WC, Salabas E, Spliethoff B, Schuth F. Low temperature catalytic pyrolysis for the synthesis of high surface area, nanostructured graphitic carbon. Chem Mater 2006;18:2086–94.
[13] Xia BY, Wang JN, Wang XX, Niu JJ, Sheng ZM, Hu MR, et al. Synthesis and application of graphitic carbon with high surface area. Adv Funct Mater 2008;18:1790–8.
[14] Journet C, Master WK, Bernier P, Loiseau A, Lamy de la Chapellw M, Lefrant S, et al. Large-scale production of single-walled carbon nanotubes by the electric-arc technique. Nature 1997;388:756–8.
[15] Thess A, Lee R, Nikolaev P, Dai HJ, Petit P, Robert J, et al. Crystalline ropes of metallic carbon nanotubes. Science 1996;273:483–7.
[16] Terrones M, Grobert N, Olivares J, Zhang JP, Terrones H, Kordatos K, et al. Controlled production of aligned-nanotube bundles. Nature 1997;388:52–5.
[17] Hanzawa Y, Hatori H, Yoshizawa N, Yamada Y. Structural changes in carbon aerogels with high temperature treatment. Carbon 2002;40:575–81.
[18] Fu R, Baumann TF, Cronin S, Dresselhaus G, Dresselhaus MS, Satcher Jr JH. Formation of graphitic structures in cobalt–nickel-doped carbon aerogels. Langmuir 2005;21:2647–51.
[19] Fu RW, Dresselhaus MS, Dresselhaus G, Zheng B, Liu J, Satcher Jr J, et al. The growth of carbon nanostructures on cobalt-doped carbon aerogels. J Non-Cryst Solids 2003;318:223–32.
[20] Maldonado-Hodar FJ, Moreno-Castilla C, Rivera-Utrilla J, Hanzawa Y, Yamada Y. Catalytic graphitization of carbon aerogels by transition metals. Langmuir 2000;16:4367–73.
[21] Hyeon T, Han S, Sung YE, Park KW, Kim YW. High-performance direct methanol fuel cell electrodes using solid-phase-synthesized carbon nanocoils. Angew Chem Int Ed 2003;42:4352–6.
[22] Lu AH, Li W, Matoussevitch N, Spliethoff B, Bonnemann H, Schuth F. Highly stable carbon-protected cobalt nanoparticles and graphite shells. Chem Commun 2005:98–100.
[23] Moreno-Castilla C, Maldonado-Hodar FJ. Synthesis and surface characteristics of silica- and alumina–carbon composite xerogels. Phys Chem Chem Phys 2000;2:4818–22.
[24] Maldonado-Hódar FJ, Moreno-Castilla C, Rivera-Utrilla J. Synthesis, pore texture and surface acid–base character of TiO_2/carbon composite xerogels and aerogels and their carbonized derivatives. Appl Catal A Gen 2000;203:151–9.
[25] Moreno-Castilla C, Maldonado-Hodar FJ, Carrasco-Marın F, Rodrıguez-Castellon E. Surface characteristics of titania/carbon composite aerogels. Langmuir 2002;18:2295–9.
[26] Muller H, Rehak P, Jager C, Hartmann J, Meyer N, Spange S. A concept for the fabrication of penetrating carbon/silica hybrid materials. Adv Mater 2000;12:1671–5.
[27] Spange S, Grund S. Nanostructured organic–inorganic composite materials by twin polymerization of hybrid monomers. Adv Mater 2009;21:1–6.
[28] Choura M, Belgacem NM, Gandini A. Acid-catalyzed polycondensation of furfuryl alcohol: mechanisms of chromophore formation and cross-linking. Macromolecules 1996;29:3839–50.
[29] Grund S, Seifert A, Baumann G, Baumann W, Marx G, Kehr M, et al. Monolithic silica with bimodal pore size distribution fabricated by self-separated sol–gel composite materials. Micropor Mesopor Mater 2006;95:206–12.
[30] Derbyshire FJ, Presland AEB, Trimm DL. Graphite formation by dissolution–precipitation of carbon in cobalt, nickel and iron. Carbon 1975;13:111–3.
[31] Oya A, Marsh H. Phenomena of catalytic graphitization. J Mater Sci 1982;17:309–22.
[32] Gupta G, Slanac DA, Kumar P, Wiggins-Camacho JD, Wang XQ, Swinnea S, et al. Highly stable and active Pt–Cu oxygen reduction electrocatalysts based on mesoporous graphitic carbon supports. Chem Mater 2009;21:4515–26.
[33] Maldonado S, Morin S, Stevenson KJ. Structure, composition, and chemical reactivity of carbon nanotubes by selective nitrogen doping. Carbon 2006;44(8):1429–37.
[34] Tuinstra F, Koenig JL. Raman spectrum of graphite. J Chem Phys 1970;53(3):1126–8.
[35] Kim TW, Park IS, Ryoo R. A synthetic route to ordered mesoporous carbon materials with graphitic pore walls. Angew Chem Int Ed 2003;42:4375–9.
[36] Wang DW, Li F, Liu M, Lu GQ, Cheng HM. 3D aperiodic hierarchical porous graphitic carbon material for high-rate electrochemical capacitive energy storage. Angew Chem Int Ed 2008;47:373–6.
[37] Xia KS, Gao QM, Jiang JH, Hu J. Hierarchical porous carbons with controlled micropores and mesopores for supercapacitor electrode materials. Carbon 2008;46:1718–26.
[38] Liu HJ, Cui WJ, Jin LH, Wang CX, Xia YY. Preparation of three-dimensional ordered mesoporous carbon sphere arrays by a two-step templating route and their application for supercapacitors. J Mater Chem 2009;19:3661–7.
[39] Liang YY, Feng XL, Zhi LJ, Kolb U, Mullen K. A simple approach towards one-dimensional mesoporous carbon with superior electrochemical capacitive activity. Chem Commun 2009:809–11.
[40] Dong XP, Shen WH, Gu JL, Xiong LM, Zhu YF, Li H, et al. MnO_2 embedded in mesoporous carbon wall structure for use as electrochemical capacitors. J Phys Chem B 2006;110:6015–9.
[41] Lee KT, Ji XL, Rault M, Nazar LF. Simple synthesis of graphitic ordered mesoporous carbon materials by a solid-state method using metal phthalocyanines. Angew Chem Int Ed 2009;48:5661–5.
[42] Zhai Y, Wan Y, Cheng Y, Shi Y, Zhang Y, Tu B, et al. The influence of carbon source on the wall structure of ordered mesoporous carbons. J Porous Mater 2008;15:601–11.
[43] Wen ZB, Qu QT, Gao Q, Zheng XW, Hu ZH, Wu YP, et al. An activated carbon with high capacitance from carbonization of a resorcinol–formaldehyde resin. Electrochem Commun 2009;11:715–8.
[44] Yuan DS, Chen JX, Tan SX, Xia NN, Liu YL. Worm-like mesoporous carbon synthesized from metal-organic coordination polymers for supercapacitors. Electrochem Commun 2009;11:1191–4.